Available online at www.sciencedirect.com
ScienceDirect
Ocean Engineering 34 (2007) 856–869
OCEAN ENGINEERING
www.elsevier.com/locate/oceaneng

Geometry of scour hole around, and the influence of the angle of attack on the burial of finite cylinders under combined flows

Yovanni A. Cataño-Lopera*, Marcelo H. García

Ven Te Chow Hydrosystems Laboratory, University of Illinois at Urbana-Champaign. 205 N. Mathews Avenue, Urbana, IL 61801, USA

Received 9 November 2005; accepted 21 March 2006
Available online 5 July 2006

Abstract

Experiments were conducted to investigate the geometry of the scour hole and flow structure around short cylinders under the action of waves alone (WA) and combined flows (CF). The study is aimed at better understanding the dynamics of isolated objects on a sandy floor under oscillatory flows as occurs in shallow water regions in coastal areas. Flow velocities within the fluid core were recorded and 3D mapping of the bottom was performed with sub-aquatic acoustic sensors. Experiments were conducted for cylinder Reynolds wave number and Keulegan-Carpenter number within the ranges $10^4 \leqslant R_e \leqslant 1.7 \times 10^5$ and $2 \leqslant KC \leqslant 71$, respectively. The present experimental evidence shows that the geometric characteristics of the scour hole (length and width) depend primarily on the Keulegan-Carpenter number (KC) and the cylinder aspect ratio ($a_r = L_c/D$). The effect of variation in the angle of attack of the flow with respect to the cylinder main axis was also investigated. Initial orientations of zero and ninety degrees were found to be stable while cylinders with intermediate initial orientations tended to orientate their main axes perpendicular to the flow direction. The final angle of orientation was found to be primarily a function of the Shields parameter, θ, and the initial angle of attack, α_i.

Keywords: Angle of attack; Combined flows; Cylinders; Objects burial; Scour hole

1. Introduction

The study of scour of sediment around objects such as pipelines and short cylinders under the action of oscillatory flows is of great importance for hydraulic and ocean engineers (Smith and Foster, 2005; Voropayev et al., 2003). Objects placed on the seabed subjected to the wave-current action may undergo partial to total burial (Voropayev et al., 1999, 2003). Burial of the object may be induced by local scour or the passage of migrating bedforms (Voropayev et al., 2003; Morelissen et al., 2003; Cataño-Lopera and García, 2005, 2006).

Earlier experimental investigations on burial of short cylinders and the effect of angle of attack of the flow with respect to the cylinder main axis were conducted by Carstens and Martin (1963) with an oscillatory sediment tunnel. Carstens and Martin (1963) used rather small cylinders and rather limited flow conditions, compared to later works by other investigators, and described self-burial of finite cylinders based on the sediment Froude number (defined as $F_r = U_m/((\gamma_s - 1)gd_{50})^{1/2}$, where U_m is the maximum value of the undisturbed orbital velocity at the bed level, γ_s is the specific gravity of the sediment, g is the acceleration due to the gravity and d_{50} is the mean diameter of the bed material). Carstens and Martin (1963) also studied the effect of variation in the angle of attack and found that the cylinder tended to rapidly orientate its main axis perpendicular to the flow direction for higher values of F_r, e.g. 11.2. Their predictive expressions apply to cases where the initial orientation is larger than 30° for cylinders ranging from 1.2 to 8.8 cm in diameter. The turning of the object is primarily due to the torque that the flow exerts on the cylinder and the central support under the cylinder serves as a pivot for turning (Carstens and Martin, 1963).

More recently, Voropayev et al. (2003) conducted experiments on burial of finite cylinders under the action of shoaling waves on a sloped bottom. They discovered that the equilibrium burial depth of the specimen was

*Corresponding authors. Tel.: +217 333 8365; fax: +217 3330687.
E-mail addresses: catano@uiuc.edu (Y.A. Cataño-Lopera), mhgarcia@uiuc.edu (M.H. García).

0029-8018/$ - see front matter © 2006 Elsevier Ltd. All rights reserved.
doi:10.1016/j.oceaneng.2006.05.001

Nomenclature

a	amplitude of the orbital motion of the water particles
a_{wc}	amplitude of the orbital motion of the water particles for the case of CF
B_{do}	initial burial depth
B_{dt}	burial depth at time t
C_w	wave celerity
D	cylinder diameter
d_{50}	mean sediment size
F_r	Froude number
f_w	wave frequency
f_{fw}	wave friction coefficient
g	acceleration due to gravity
H_w	wave height
h	water depth
KC	Keulegan–Carpenter number
k	wave number
k_s	surface mean roughness height of the cylinder
L_c	length of the cylinder
L_w	wavelength
L_{st}	total length of the scour hole
L_{sd}	length of the downstream side of the scour hole
L_{su}	length of the upstream side of the scour hole
p	pressure
R_e	cylinder Reynolds wave number
R_{ew}	Reynolds wave number
S_o	stroke at the plate of the wavemaker measured in cm
T	time scale of burial process
T_w	peak wave period
T^*, T_s	dimensionless time scale
t	time
U	mean flow velocity of the current
U_c	velocity of the current at the center of the cylinder
U_{fm}	friction velocity in the case of currents
U_m	maximum value of the orbital velocity of water particles at the bottom
U_r	Ursell number
U_w	orbital velocity of water particles
U_{mc}	maximum value of the orbital wave-current velocity at the bottom
U_{wc}	effective wave-current velocity in CF
W_s	width of the scour hole
x, y, z	spatial coordinates
α_i	initial orientation of the cylinder main axis with respect to the wave direction
α	orientation of the cylinder main axis with respect to the wave direction
β	angle of interaction between the waves and the current
γ	specific gravity of water
γ_c	specific gravity of cylinder
γ_s	specific gravity of sediment
θ	Shields shear stress
θ_{cr}	critical Shields shear stress
ν	kinematic viscosity of fluid
ρ_c	density of cylinder
ρ_s	density of sediment
σ	angular frequency of waves
σ_{dg}	standard deviation of the particle sand distribution
τ	bed shear stress
τ_∞	bed shear stress for the undisturbed flow
φ	internal friction angle of sand

determined by a combined effect of the Keulegan–Carpenter number KC (defined as $KC = U_m T_w / D$, where T_w is the wave period, and D is the cylinder diameter) and the Shields Parameter θ. Later, Cataño-Lopera and García (2005, 2006) conducted experiments including the case of CF and proposed an estimator of equilibrium burial depth, B_d, which is determined by the combined effect of KC, θ, and the ratio of the wave velocity to the net wave-velocity.

The evolution of the scour hole around pipelines has been studied experimentally under waves by Sumer and Fredsoe (1990) and under combined flows by Sumer and Fredsoe (1996). Sumer et al. (2001) and Sumer and Fredsoe (2002a, b) summarize results from experiments on self-burial of pipelines under currents, waves alone, and waves plus currents. The latter authors report that the main parameter for describing the scour hole is the Keulegan–Carpenter number. Extensive numerical investigations on the scour beneath offshore pipelines have also been conducted by Hansen (1992), Li and Cheng (1999a, b), Bros (1999), Smith and Foster (2005), Liang et al. (2005).

Extensive field and laboratory investigations have been conducted during the last couple of decades due to the naval interest on the behavior and burial of short cylinders under the action of oscillatory flows. Little attention has been paid to the case of short cylinders except for a rather limited set of experiments conducted by Voropayev et al. (2003). In their work, Voropayev et al. (2003) described the evolution over time of the length of the scour hole around short cylinders under shoaling waves on a sloped bottom.

In the present study, the scour hole at equilibrium conditions was investigated. The geometry of the bottom around the object was described with the help of a digital photo camera and a set of sub-aquatic acoustic sensors. Data corresponding to more than fifty experiments of the geometry of the scour hole combining the cases of waves alone and combined flows are reported. Results showed that both the width and length of the scour hole depend primarily on the KC number and the cylinder aspect ratio, a_r. The latter finding was possible due to the use of a set of cylinders with aspect ratios ranging from 2 to 4. Table 1

Table 1
Experimental ranges of flow parameters

Hydraulic conditions	T_w (s)	H_w (cm)	U_m (cm/s)	U (cm/s)	U_c (cm/s)	$\frac{U_c}{U_c+U_m}$	KC	R_{ew}	R_e	θ	W_s/D	L_{st}/D	L_{sd}/D
WA Min.	1.5	10	18.8	0	0	0	2.4	1.1×10^4	1.0×10^4	0.08	2.7	1.8	0.8
Max.	6.9	31	55.4	0	0	0	63.5	2.6×10^5	1.4×10^5	0.52	6.3	8.3	7.2
CF Min.	1.4	10	17.1	17.3	15.2	0.23	3.0	7.8×10^4	2.1×10^4	0.20	3.0	1.6	1.8
Max.	5.9	29	50.7	17.3	15.2	0.47	71.4	6.1×10^5	1.7×10^5	0.66	6.3	7.7	6.3

presents a summary of the characteristics of the tested cylinders.

In this study, the influence of the angle of attack of the flow with respect to the cylinder's main axis on the equilibrium burial depth was also investigated. Results suggest that cylinder burial increased for increasing angle of attack, i.e. being a minimum for zero degrees and reaching maxima for ninety degrees.

The main purpose of the present work is to aid in the understanding of the main processes responsible for the burial of finite-length cylinders under wave plus current dominated environments.

2. General analysis

Similar to the case of burial depth, it is possible to show from dimensional analysis that under combined waves plus currents the scour hole characteristics around finite cylinders can be represented in the dimensional form

$$S_g = F(D, L_c, \rho_c, k_s, d_{50}, \rho_s, \sigma_{dg}, t, U_m, U, T_w, \nu, g, \alpha_i, B_{d0}), \tag{1}$$

where S_g refers to scour geometry and may represent scour depth, length or width of the scour hole around the cylinder.

According to some authors, if a body is sufficiently heavy and does not move under the wave action, then the body's specific gravity, γ_c, can be neglected (Voropayev et al., 1999; Cokgor, 2002; Voropayev et al., 2003). Certainly this may be the case in the determination of the geometry of the scour hole around the cylinder but not completely true for the case of self-burial of the cylinder. Recent experimental evidence suggests that cylinder density plays an important role on the equilibrium burial depth of the cylinder (Cataño-Lopera and García, 2005, 2006).

Experimental evidence also shows that if the surface roughness, k_s, of the cylinder is very small corresponding to that of a smooth surface, then k_s can also be neglected (Voropayev et al., 2003). If the bed material is uniformly sized then its standard deviation, σ_{dg}, could also be discarded.

Combining the remaining parameters in Eq. (1) the following dimensionless form can be deduced,

$$S_g = F(a_r, R_e, R_{ew}, KC, \theta, T^*, \gamma_c, \alpha_i, B_{d0}/D, U/(U_m+U) \text{ or } U_m/(U_m+U)), \tag{2}$$

where $a_r = L_c/D$ is the cylinder aspect ratio. Notice that in the case of vanishing currents, i.e. $U = 0$, Eq. (2) reduces to the case of waves alone.

3. Experimental setup and test conditions

3.1. Apparatus

Experiments with progressive waves were conducted in a large tilting wave-current flume of dimensions 49 m × 1.83 m × 1.22 m. This facility has a steel floor and Plexiglas sidewalls to provide full optical access. The slope of the flume for the experiments was set to zero. For combined flow experiments, a re-circulating current was introduced via a diffuser located at the bottom of the tank, underneath the wavemaker paddle. The arrangement allowed variable discharge, with a total capacity of 0.22 m^3/s. To control the injected discharge it was necessary to use a constant head tank and a pump. This was enough to generate a current of approximately 0.2 m/s. A piston type wave maker was used to generate regular waves. The wave generator consists of a vertical steel plate that is driven by a hydraulic ram. A schematic diagram of the experimental facility is shown in Fig. 1.

A sand bed (24 m long, 1.83 m wide and 0.31 m deep) was placed at the bottom of the central region of the tank. The upstream edge of the bed started approximately 3.6 m from the mean position of the wavemaker paddle.

At the downstream end of the flume the wave motion was absorbed by a beach covered by a riprap blanket that is 6.0 m long and 1.1 m high. In experiments with relatively small and regular progressive surface waves, the reflection coefficient was estimated to be less than 12%, based on height envelope considerations. As wave amplitude and wave period increased, the efficiency of the beach to dissipate energy was reduced. Range of experimental flow conditions and flow parameters are listed in Table 1.

In order to measure wave amplitude and period an acoustic sensor model SU7110 with a 12 Hz sampling rate and ±0.8 mm vertical resolution was utilized. This sensor was mounted on a movable carriage located on rails at the top of the wave flume. The underlying velocity field was measured using a standard three-component acoustic Doppler velocimeter (ADV). This system allows measurements of the three velocity components simultaneously at a data collection frequency of 25 Hz within a measuring

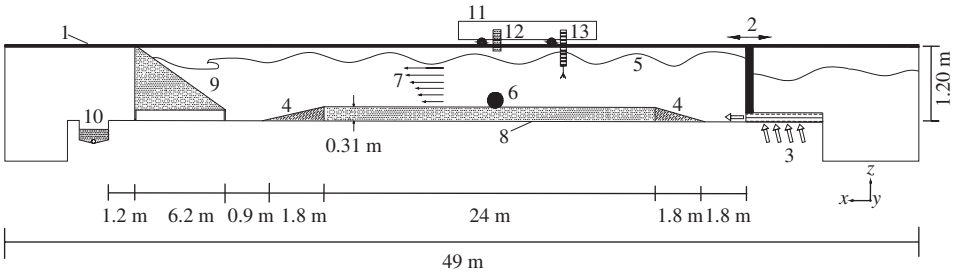

Fig. 1. Schematic diagram of the experimental setup: 1. wave flume; 2. wavemaker paddle; 3. injection of current; 4. wooden ramp; 5. waves; 6. cylinder; 7. superimposed current; 8. sandy bed; 9. beach; 10. sediment trap; 11. movable carriage; 12. water surface acoustic sensor; 13. ADV probe.

Table 2
Properties of model cylinders

Cylinder Material	Conc. 1	Conc. 2	Conc. 3	Conc. 4	Conc. 5	Alum. 1	Alum. 2	Steel 1	Steel 2
Diameter (cm)	25.4	20.3	15.2	12.5	10.2	8.6	8.6	5.1	7.6
Length (cm)	102	81.3	30.5	25.4	20.3	26.2	35.1	20.3	20.3
Aspect ratio, a_r	4.0	4.0	2.0	2.0	2.0	3.0	4.0	4.0	2.7
Specific gravity, γ_c	2.0	2.0	2.3	2.3	2.3	2.7	2.7	7.85	7.85
R. height, k_s (mm)	0.8	0.8	0.8	0.3	0.8	0.1	0.1	0.3	0.3

cylindrical volume of approximately 0.1 cm^3 (Snyder and Castro, 1999). The ADV was attached to a frame with the capability of vertical z-axis and transversal y-axis displacements. The frame was mounted on a movable carriage allowing motion in the third spatial component, i.e. along the main axis x of the flume.

Information on bottom topography of the scour hole around the cylinder was collected using a 32-composite-element array of sub-aquatic acoustic sensors (developed by SeaTek, Inc.). This instrument allows resolution of the order of ± 2 mm in the vertical. The array of sensors was attached to a frame that allowed vertical displacement which in turn was mounted to a movable carriage which also supported the ADV. Top photographs of intermediate and final configurations of the scour hole around the cylinder were taken with the help of a standard digital camera.

3.2. Measuring procedure

In the present tests, the measuring section was located approximately 20 m downstream of the wavemaker paddle along the centerline of the flume to allow proper flow development. The sand material used had a mean diameter of $d_{50} = 0.25$ mm and a standard deviation of $\sigma_{dg} \approx 1.28$. The internal angle of repose of the sand was $\varphi \approx 32.5^\circ$ obtained from a tri-axial test, and the porosity of the sand was experimentally estimated to be $\lambda_p = 0.3$. In total, nine model cylinders were employed in the present tests. Five cylinders were made of concrete, two were made of steel and other two cylinders were of aluminum. The geometric characteristics and materials of the model cylinders are presented in Table 2. The mean water temperature of the water during the experiments was measured to be about 21 °C. The corresponding kinematic viscosity at this temperature was estimated to be $\nu = 9.8 \times 10^{-7}$ m^2/s.

For studying the geometric characteristics of the scour hole at equilibrium conditions and the effect of the angle of attack of the flow with respect to the cylinder, single model cylinders were gently placed at the center line over the sand bed. The sand bed was leveled horizontally before each experiment. The working water depth at still conditions was set to 56 cm on the average. The initial burial depth of the cylinder was estimated to be $B_{do} \approx 0.3$ cm in the case of the concrete and aluminum cylinders and $B_{do} \approx 0.4$ cm in the case of the steel cylinders.

To track the burial of a model cylinder, an acoustic Doppler velocimeter (ADV) was employed by placing its tip right above the top of the cylinder's center. The distance from the sensor to the top of the cylinder was recorded as a function of time. The ADV has vertical resolution of the order of ± 1 mm allowing accurate burial depth measurements. The ADV probe was also utilized for recording vertical velocity profiles.

For studying the effect of cylinder orientation on the cylinder settlement and geometry of the scour hole, cylindrical models were placed on the bed at various angles of orientation α_i (0°, 30°, 45°, 60°, 75°, 90°; where 90° corresponds to the main cylinder axis oriented perpendicularly with respect to the flow direction), and with certain initial burial depth B_{d0}. Initial and final angles of orientation were obtained with the help of top photographs, triangular rulers, and a 360° protractor. Duration of each experiment was approximately 120 min. Normally after 2 h, formation of bed features like sandwaves occur and then the cylinder burial is no longer governed by the so called local scour (Cataño-Lopera and García, 2005).

3.3. Background flow conditions

Although the motion of the wavemaker is sinusoidal, as the waves enter the sand bed zone they steepen and become nonlinear. The resulting nonlinearities are due, in part, to the rapid decay of the water level from 87 cm before the first ramp (from right to left in Fig. 1) down to 56 cm over the sand bed. If the wave frequency f_w is high enough then the resulting nonlinearities are small and linear theory is still applicable.

For the case of combined wave-current motion, the fluid-orbital amplitude can be calculated as

$$a_{wc} = \frac{T_w}{2\pi}\sqrt{U_w^2 + \pi^2 U_w^2 + 2\pi U_w U|\cos\ \beta|}, \tag{3}$$

where U is the vertically-averaged velocity of the unidirectional current and β is the angle of interaction between the waves and the current (it is zero in the present study). The wave-current velocity can be calculated as

$$U_{wc} = \sqrt{U_w^2 + U^2 + 2U_w U|\cos\ \beta|}, \tag{4}$$

Notice that from equations three and four, a_{wc} and U_{wc} become a and U_w, respectively, as in the case of waves alone.

It is worth noticing that as both, the wave period, T_w, and the paddle stroke at the wavemaker, S, increase, the nonlinearities at the surface and in the velocity profiles of the underlying flow field are noticeable more and more. For this reason velocity profiles away from the cylinder were measured directly by using an ADV probe, especially for the cases in which high nonlinearities were visually observed. Velocity time series were recorded over 50 wave periods along the vertical. The nearest measurement to the bottom was taken at a distance of approximately 1 cm off the bed. Having the vertical velocity profile, the value of the velocity at the bed level was then estimated. This velocity is important for computations of flow parameters such as the wave Reynolds number and the Shields parameter. On the other hand, estimation of the velocity at the center of the cylinder was necessary for the computation of the KC number and the cylinder Reynolds number, R_e. Records of surface profiles and flow velocities allowed the determination of the wave period after computing the fast Fourier transform FFT of the signal. Fig. 2 shows typical velocity time series recorded with the ADV probe.

4. Computation of the dimensionless parameters

A list containing the ranges for the dimensionless flow parameters used in the present study is presented in Table 1. The definitions hereafter correspond to the case of waves alone.

The Keulegan–Carpenter number is computed as

$$\mathrm{KC} = \frac{U_m T_w}{D}. \tag{5}$$

The cylinder Reynolds wave number is defined as

$$R_e = \frac{U_m D}{\nu}. \tag{6}$$

The case of combined flows is straight forward after noticing that U_m has to be changed for $U_m + U_c$, where U_c is the undisturbed current velocity at the center of the cylinder, in Eqs. (5) and (6).

In a similar fashion, the Reynolds wave number is computed as

$$R_{ew} = \frac{U_m a}{\nu}. \tag{7}$$

The Shields parameter herein is computed using the widely used formula of Swart (1974), that is

$$\theta = \frac{1}{2} f_{fw} \frac{U_m^2}{(\gamma_s - 1) g d_{50}}, \tag{8}$$

where f_{fw} is the friction factor which for rough turbulent flow reads as

$$f_{fw} = 0.3 \quad \text{for } a/2.5d_{50} \le 1.57, \tag{9a}$$

$$f_{fw} = 0.00251\ \mathrm{Exp}(5.21(a/2.5d_{50})^{-0.19}) \quad \text{for } a/2.5d_{50} > 1.57 \tag{9b}$$

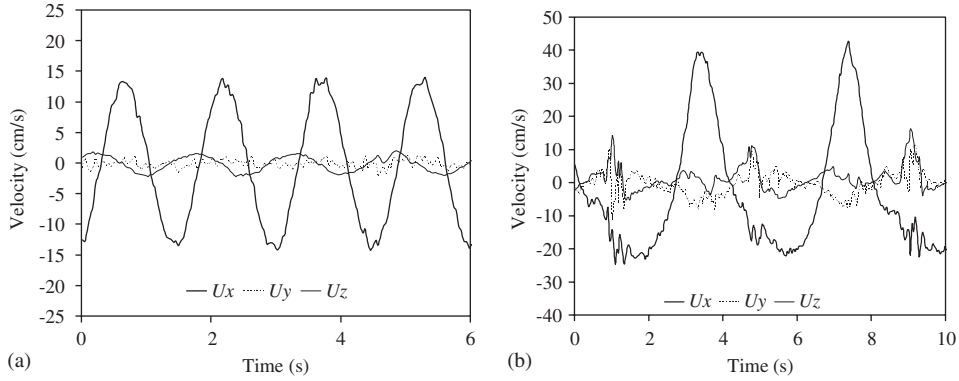

Fig. 2. Typical longitudinal u_x; transverse u_y; and vertical u_z; flow velocities components at 1 cm from the mean level of the bottom away from the cylinder. Case of waves alone with (a) $T_w = 1.5$ s, $H_w = 15.5$ cm, $L_w = 3.5$ m, $h = 56$ cm at 2 cm off the bottom; (b) $T_w = 4.1$ s, $H_w = 16.7$ cm, $L_w = 9.4$ m, $h = 56$ cm at 30 cm off the bottom.

And the friction factor f_{fw} is computed considering only the skin friction component. Notice in Eqs. (7) and (8) that for combined flow U_m needs to be replaced by $U_m + U$, and a_{wc} should be used instead of a in Eq. (9).

Normally, for the tested flow conditions, migrating ripples formed during the first two to four minutes of the experiment. The ripples affect the approaching velocity field around the object. Strictly speaking, to compute a more realistic friction factor, the friction contribution associated to bed forms has to be added to the skin friction component. Nevertheless, only the skin friction is used in this study for comparison purposes since previous empirical formulae relied on it (Sumer and Fredsoe, 2002a, b; Voropayev et al., 2003).

5. Experimental results

Two kinds of experiments were conducted: first, waves alone and second, combined waves plus currents. In both cases, the subsequent evolution over time of the initially flat bed around the cylinder, as well as, the burial of the body was measured. In total, about 130 experiments under WA and 100 under CF were conducted for studying the effect of the angle of attack on the cylinder burial. Among the total set of experiments about 50 with $\alpha_i = 90^\circ$ were chosen and reported here for the study of the geometry of the scour hole around the cylinder.

5.1. Geometry of the scour hole around the cylinder

The lee-wake erosion, related to the strong turbulent patterns surrounding the cylinder due to the back and forth motion of the waves, seems to be the most responsible agent for the formation and shape of the scour hole around the cylinder. Fig. 3 shows the definitions associated to the characteristics of the scour hole. Depending on the acting wave-current climate, the influence of wakes may be present up to several cylinder diameters up and downstream the cylinder. The KC number plays a significant role on the final scour depth around cylindrical structures like piers (Sumer and Fredsoe, 2001), pipelines (Sumer and Fredsoe, 1990, 1996; Sumer et al., 2001) and finite-length cylinders (Sumer and Fredsoe, 2002a, b; Voropayev et al., 2003; Cataño-Lopera and García, 2006). The role of KC on the scour and burial process has been supported by the observations made in the present study. In this study, besides the effect of the KC number, it has been determined that the cylinder aspect ratio, a_r, also plays a significant role on the shape and size of the scour hole. Either under WA or CF, the lee-wake effects extend downstream more than upstream of the body. As a consequence, the length of the scour hole downstream of the cylinder, L_{sd}, is usually larger than its counterpart, L_{su}. Under WA, this effect is more apparent as the wave period, T_w, and paddle stroke, S, increase with corresponding increasing wave nonlinearities (e.g. Fig. 2b).

Fig. 4 shows a plot of measured dimensionless scour hole width (W_s/L_c) as a function of KC for cylinders with their main axis orientated 90° with respect to the flow direction. Among the dimensionless parameters listed in Eqs. (5–8), KC produces the smallest scatter. In both cases, the scour width ranges approximately from 1.3 to 2.5, with a mean

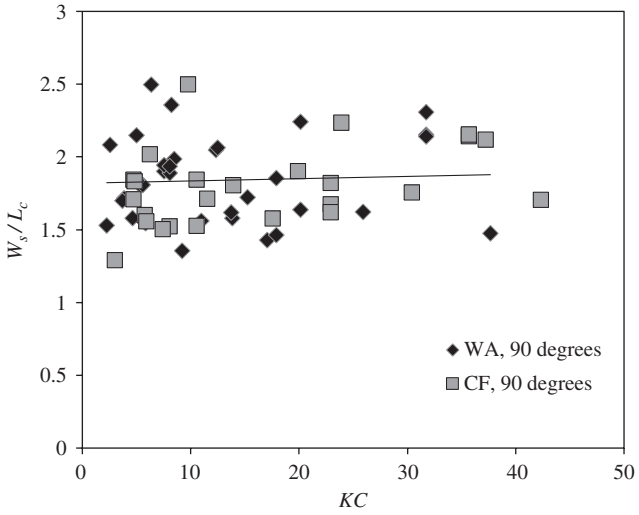

Fig. 4. Equilibrium dimensionless width of scour hole W_s as a function of the KC number.

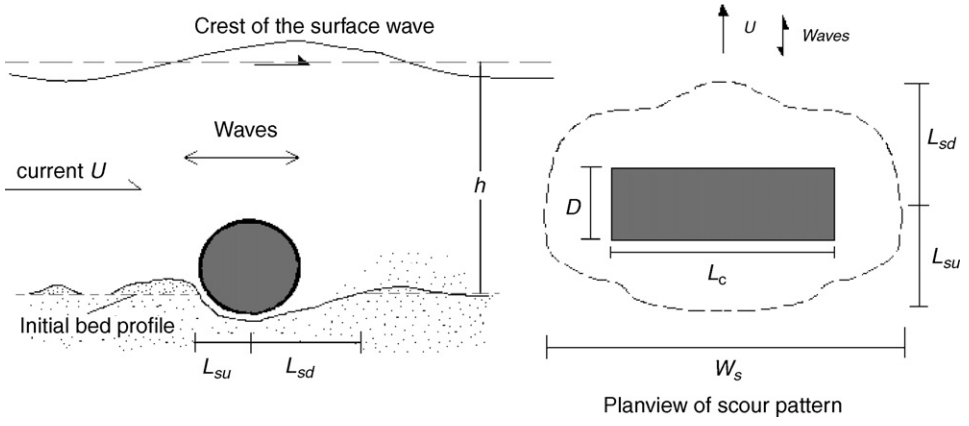

Fig. 3. General schematic diagram of the geometric dimensions for 2D scour oscillatory flows.

value of 1.8 regardless the KC number. Cylinder aspect ratio and density seem not to affect the width in an appreciable manner.

As seen in Fig. 3, the total equilibrium length of the scour hole can be divided in two parts. One for the downstream side L_{sd}, and one for the upstream region L_{su}. A plot of the measured data of L_{sd}/D against KC is shown in Fig. 5. Notice that L_{sd}/D increases with increasing KC; and so does the upstream length, although not shown here. The best fit is obtained by the following relationship

$$\frac{L_{sd}}{D} = 0.75\,\mathrm{KC}^{0.56}, \tag{10}$$

with a correlation coefficient of $\rho^2 = 0.73$ after combining both data sets, WA and CF.

Notice in Fig. 5 that both data sets share a common region, and there is not significant distinction between waves alone and combined flows regardless cylinder characteristics.

In a similar fashion, the total dimensionless length of the scour hole increases as KC increases (Fig. 6). Once more, the best law fit of the measured data set is given by a power relationship given by

$$\frac{L_{st}}{D} = 1.46\,\mathrm{KC}^{0.44} \tag{11}$$

with a correlation coefficient of $\rho^2 = 0.74$ after combining both data sets, WA and CF.

The upstream portion of the scour hole, i.e. L_{su} can be readily calculated after subtracting Eq. (10) from Eq. (11).

A comparison of the measured data, along with a plot representing Eq. (11), and existing predictive formulae in the case of short cylinders over a sloped bottom under shoaling waves (Voropayev et al., 2003) and for pipelines under waves (Sumer and Fredsoe, 2002a, b) is presented in Fig. 7. The expression proposed by Sumer and Fredsoe (2002a, b) read as

$$\frac{L_{st}}{D} = 0.35\,\mathrm{KC}^{0.65} \tag{12}$$

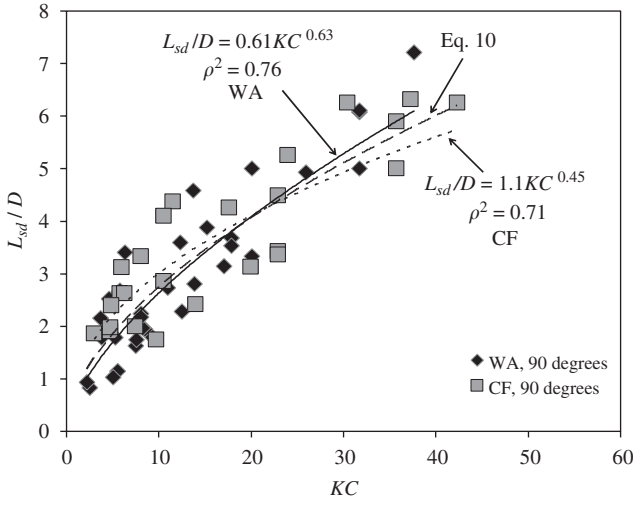

Fig. 5. Measured L_{sd}/D as a function of KC.

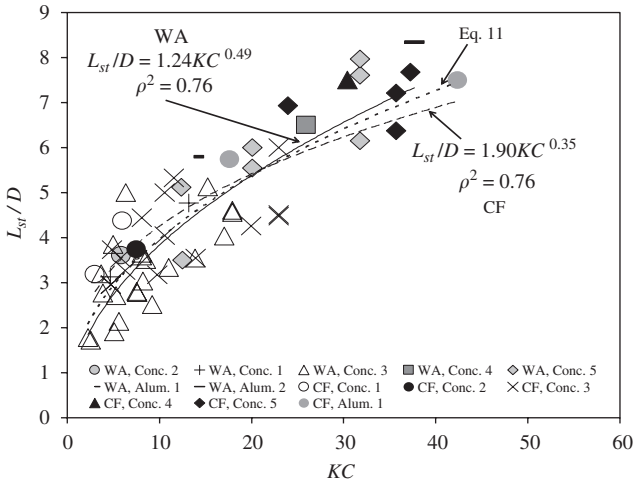

Fig. 6. Measured L_{st}/D as a function of KC.

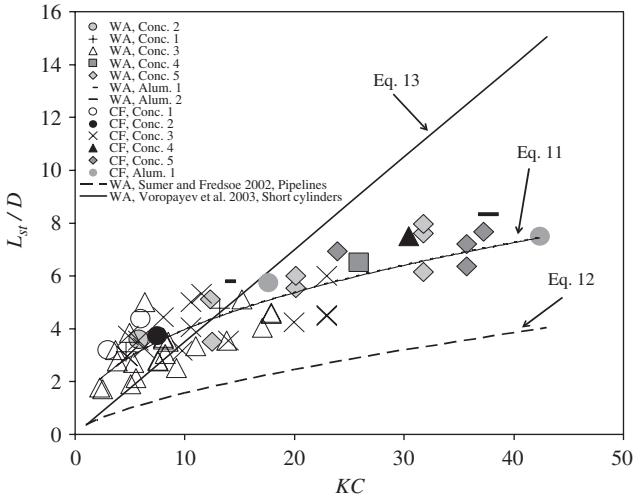

Fig. 7. Dimensionless length of the scour hole as a function of KC. Comparison with existing empirical formulae.

and the expression proposed by Voropayev et al. (2003) reads as

$$\frac{L_{st}}{D} = 0.35\,\mathrm{KC}. \tag{13}$$

Notice in Fig. 7 that Eq. (12) under-predicts by far the length of the scour hole. On the other hand, notice that Eq. (13) is a linear relationship that can be considered somewhat less realistic than 'power' relationships of the form (11) and (12). The particular linear shape of Eq. (13) found by Voropayev et al. (2003) may be attributed to the fact that: (1) it corresponds to different experimental conditions, i.e. sloped bottom under shoaling waves, compared to the present study. (2) Eq. (13) is based apparently in a rather limited data set, since the referred authors report only eight experimental values and for KC < 25.

Since Eq. (11) still shows considerable data scatter as seen in Fig. 7, it is desirable to find an expression that

performs better. A way to achieve this goal would be to consider the inclusion of other dimensionless parameters as suggested by Eq. (2) in the analysis. After trying different setups of a modified version of Eq. (11), it has been observed that inclusion of R_e, R_{ew}, θ, T^*, or B_{d0}/D did not improve the quality of the predictions; and even in some cases it worsened. Among the remaining parameters, α_i is directly discarded from the present analysis since Eq. (11) refers to the case in which $\alpha = \alpha_i = 90^\circ$. The effect of the cylinder specific gravity, γ_c, seems to be particularly weak. As seem in Figs. 4–7, both data sets, WA and CF, are intermingled. So, the relative effect of the wave (or current) to net wave-current velocity, i.e. the last couple of terms in Eq. (2), can also be disregarded from the analysis. At this point the only remaining term in Eq. (2) is the cylinder aspect ratio, a_r. This makes sense since one would expect that the geometric dimensions of the scour hole, in particular its length, to be affected by the cylinder length. For instance, in the case of two cylinders with identical diameters but with different lengths, it is expected that the equilibrium length of the scour hole associated to the longer cylinder is larger than the associated to the shorter cylinder. In the case of the longer cylinder, the lee-wake is capable of transporting more sediment to farther distances away from the body.

The overall data scatter is then reduced if a_r is introduced properly in the analysis. In this way, a modified version of Eq. (11) after including a_r, reads as

$$\frac{L_{st}}{D} = \frac{3}{4} a_r^{3/10} \mathrm{KC}^{3/5} \tag{14}$$

where the correlation coefficient has been slightly increased up to $\rho^2 = 0.80$. Fig. 8 shows measured values and predicted values using Eq. (14) and other existing empirical formulae.

KC plays a more important role than any other dimensionless parameter in Eq. (2) on the determination of the horizontal dimensions of the scour hole. This can be understood by keeping in mind that KC is associated to the lee-wake effects related to the oscillatory motion of the flow. The lee-wake is precisely the most important factor in the transport of the re-suspended sediment away from the body. The strength of the flow is reflected in the total length of the lee-wake via the orbital amplitude of the water particles, a. The latter is associated with the distance from the body at which the sediment captured and transported in suspension is deposited. It is precisely the ratio of a/D that builds up the KC number via $\mathrm{KC} = 2\pi a/D$, which is an alternative expression of Eq. (5).

The fact that both data sets, WA and CF, share the same region regardless of cylinder properties is of great practical importance since the expressions herein obtained can be applied with certain confidence in quick estimation of scour hole geometry regardless the type of flow.

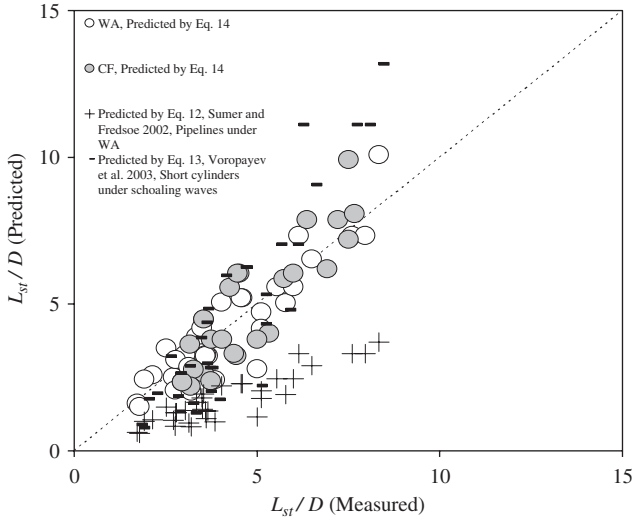

Fig. 8. Equilibrium dimensionless length of the scour hole as a function of KC. Comparison between predictive equation (14) and existing empirical formulae.

5.2. Effect of angle of attack on scouring and burial

The angle of attack is another influencing factor on the equilibrium burial depth of the cylinder (upper left in Fig. 9a). In particular, this is a very important parameter since, generally in the field the cylinder may be placed at different angles, in particular when the cylinder is thrown

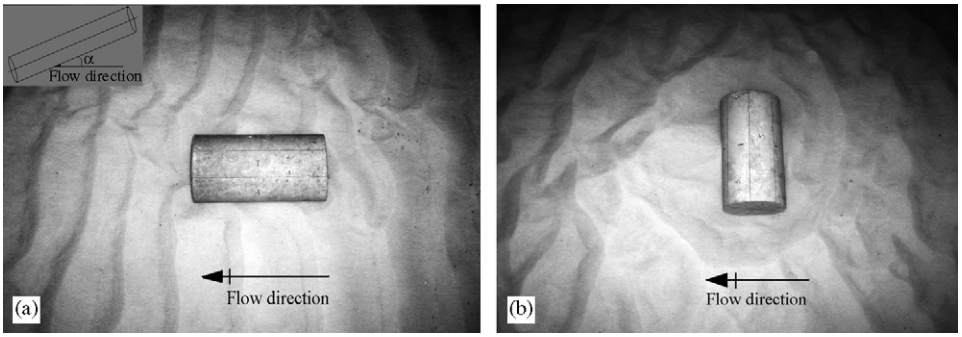

Fig. 9. Effect of the angle of attack on the scour and burial for similar hydraulic conditions under WA. (a) Upper left: Schematic diagram of angle of attack; $\alpha = 0^\circ$, (b) $\alpha = 90^\circ$. Cylinder 3 in Table 2.

from a boat implying no control of the inclination and final position of the body with respect to the acting flow. Furthermore, a cylinder may be exposed to flows varying constantly in direction from event to event. So far the effect of changes in the wave climate has been documented to some extent in the case of pipelines (Sumer and Fredsoe, 2002a, b). Numerical investigations include Hansen (1992) while experimental studies include Mao (1988) for pipelines under steady currents.

Both numerical and experimental evidence suggest that, in the case of pipelines, the scour depth under the pipeline decreases with decreasing angle of attack. This coincides with the observations from the present study where it has been noticed that the cylinder burial is larger for the case of larger orientation angles, i.e. for angles approaching 90°. This may be attributed to the fact the vortex shedding around the cylinder induced by the oscillatory motion becomes more pronounced with increasing angle of attack, e.g. for $\alpha \to 90°$, as commented by Sumer and Fredsoe (2002a, b). It is easy to understand this by noticing that larger angles of attack means more body surface to be exposed to the main direction of the flow, i.e. in the x-direction. It is precisely in the x-direction that the flow turbulence and vortex shedding are higher when compared to the transversal y and vertical z directions. The more area of the body exposed to the flow the more perturbation on the flow field. Consequently, the sediment re-suspension and transport away from the body are enhanced leading to more scour and burial (Figs. 10a and b).

Figs. 10a and b show measured data of relative burial depth as a function of final α_f and initial α_i angles of attack for WA and CF. In such plots it is observed that burial depth increases as α increases. Continuous lines in Figs. 10a and b denote fitted data trends corresponding to particular values of initial orientation. Notice also that regardless the initial angle of attack, α_i, the cylinder tends to turn to a final state where $\alpha_f > \alpha_i$. The cylinder specific gravity also plays an important role. Under similar hydraulic conditions, denser cylinders like steel made underwent smaller rotations than lighter cylinders regardless the initial orientation. This is evident by looking at the trends corresponding to lighter cylinders, e.g. concrete, compared to those of heavier cylinders. The denser ones are characterized by having milder slopes than those of lighter cylinders. In addition, observe that for initial orientations of zero and ninety degrees the cylinders did not turn, regardless the cylinder properties. This non-rotation behavior is expected when symmetrical conditions of the flow and sediments around the cylinder are present.

Figs. 11a and b show plots of final angle of attack as a function of the Shields parameter, θ, and the initial angle of attack, α_i. Similar plots are obtained when KC is used instead of θ but with weaker correlation. It seems that θ is more influential than KC over the rotation process. While

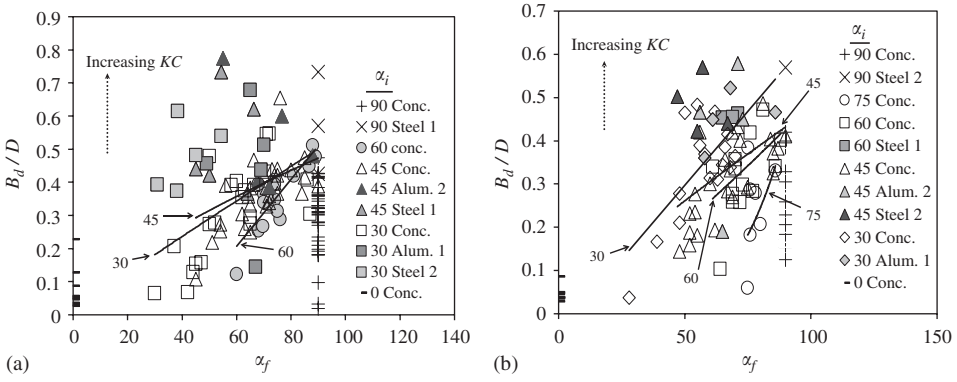

Fig. 10. Relative equilibrium burial depth as a function of the final and initial angles of attack. (a) for WA, (b) for CF.

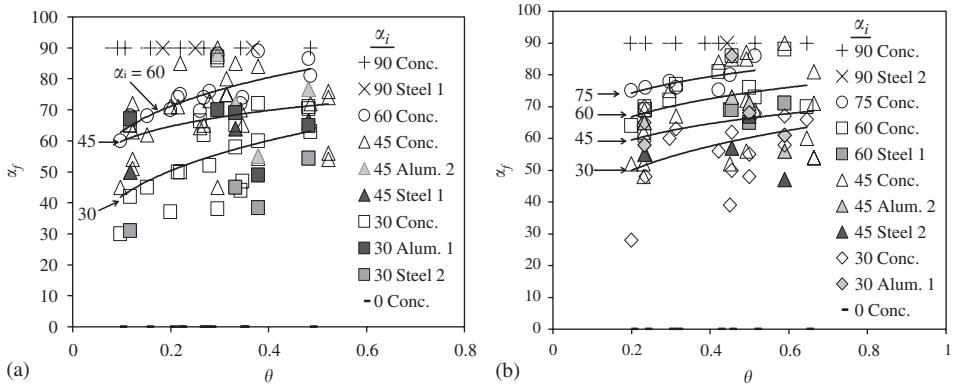

Fig. 11. Final angle of attack as a function of the Shields parameter θ and the initial angle of attack α_i: (a) for WA, (b) for CF.

KC can be more important in the process of transporting material away from the body (hence turning to be more determinant on the scour hole geometry), θ, better accounts for the local acceleration of the flow around the body which in turns enhances the excavation and re-suspension of sediment around the body.

It was observed that all cylinders tended to increase their orientation regardless of cylinder properties and initial orientation. For flows with higher θ, it is possible that cylinders with smaller α_i (e.g. 30°) end up with their main axis oriented perpendicular to the flow direction (i.e. $\alpha_f = 90°$) which is especially evident for the case of lighter cylinders (empty triangles in Fig. 11a and b). These observations are in agreement with the results obtained by Carstens and Martin (1963). These authors noticed that for sediment Froude numbers, F_r, high enough (e.g. 11.2, under which ripples did not form) and for $\alpha_i > 30°$ the cylinder turned rapidly to $\alpha_f = 90°$. In addition, an ordinary scour hole developed with accompanying cylinder settlement at basically the same rate as a cylinder placed with α_i.

Notice also in Figs. 11a and b that for WA and CF the fitted trends corresponding to different values of α_i are positive and semi-parallel. It was also observed that the predictive equation for equilibrium burial depth proposed by Cataño-Lopera and García (2006) seems to account reasonably well for cylinders with final orientations of approximately $\alpha_f > 80°$. Such equation reads as

$$\frac{B_d}{D} = \frac{6}{25}\left(\frac{U_m}{U_m + U_c}\right)(\theta\,\mathrm{KC})^{2/5}. \quad (15)$$

In summary, results from the present study suggest that the final angle of attack will depend on the compromise among several factors: the burial time scale, the strength of the flow, the density, and aspect ratio of the cylinder. For instance, a flow may be strong enough to cause a lighter cylinder to rotate to a final angle of 90°, but the same flow might not affect a denser cylinder. This can be attributed to the denser cylinder being buried faster, thus not allowing enough time to produce any further rotation. On the other hand, the aspect ratio has been observed not to play a significant role in the turning process.

5.3. Dynamics of the scour hole pattern around the cylinder: a case of study

5.3.1. Evolution of scour hole

A particular experiment was chosen to describe the evolution over time of the scour hole around a partially buried cylinder. The burial of the cylinder is controlled by two processes: one occurring in the first stages of the experiments where local scour is dominant, and a second process associated with the evolution of bedforms (i.e. ripples and sandwaves). Ripples are common bottom features that appear under unidirectional and oscillatory flows and form during the first couple minutes of the experiments. These structures have lengths and heights of the order of 10–30 cm and 2–6 cm, respectively. Sandwaves are sea features much larger than ripples with vertical and horizontal scales of the order of tens of centimeters and tens of meters, respectively. Sandwaves develop normally after a couple hours of the experiments if starting from flat bed conditions.

Local scour occurs when the cylinder dimensions are similar or higher than the surrounding bedforms. Under local scour, the scour hole varies in size and shape during the first stages of the run. At first, scour fronts form at both edges of the cylinder and travel towards its center leaving a span shoulder shorter and shorter with time. At a certain point, the underlying soil supporting the cylinder collapses due to general shear failure (Cataño-Lopera and García, 2006). This process might repeat itself until no more sinking is present, whenever the flow is not strong enough to excavate sediment from underneath the cylinder and carry it away. At the same time, scour gaps develop down- and upstream of the cylinder. Normally the downstream length is larger than its upstream counterpart. Under waves alone this happens primarily due to the non-symmetric wave velocity distribution. Normally, orbital velocities are larger in the direction of wave propagation which is often referred as Stokes's drift. Fig. 12 shows the temporal evolution of the scour hole when local scour is dominant. In this particular experiment, it was observed that local scour occurred approximately within the first 120 min.

Starting from flat bed conditions, bottom surveys were gathered every 30 min from 0–120 min. Subsequent surveys were performed at $t = 180$, 240, 360, and 3000 min, respectively. The evolution of the scour hole is described as follows: during the first 30 min, the scour hole developed while simultaneously an important portion of the final burial depth took place. A deep central gap was developed, accompanied by two sediment pipe-like protuberances formed at the downstream side of the cylinder ($t = 30$ min in Fig. 12). Notice that the two protuberances are located near the edges of the body. The extension of scour gap extended already up to several cylinder diameters. From 60 to 90 min it was observed a continuous deepening and widening of the scour hole around the cylinder (Fig. 12). Notice that the cylinder diameter is larger than the horizontal and vertical dimensions of the surrounding ripples. For this reason, ripples did not interfere with the scour hole. During this time the two sediment protuberances seem to migrate downstream primarily caused by their continuous loosening of bed material. At $t = 120$ min, the scour hole has practically reached its equilibrium shape and size (Fig. 12). At this point the two sediment protuberances are still present, although smaller than in the previous instances. From this point on, both burial and scour hole geometry barely change until approximately $t = 240$ min, when sandwaves start forming. This is manifested by the presence of larger ripples in the far downstream region of the cylinder. Sandwaves and ripples may coexist under certain flow conditions. Normally, larger ripples are superimposed to the crest of the

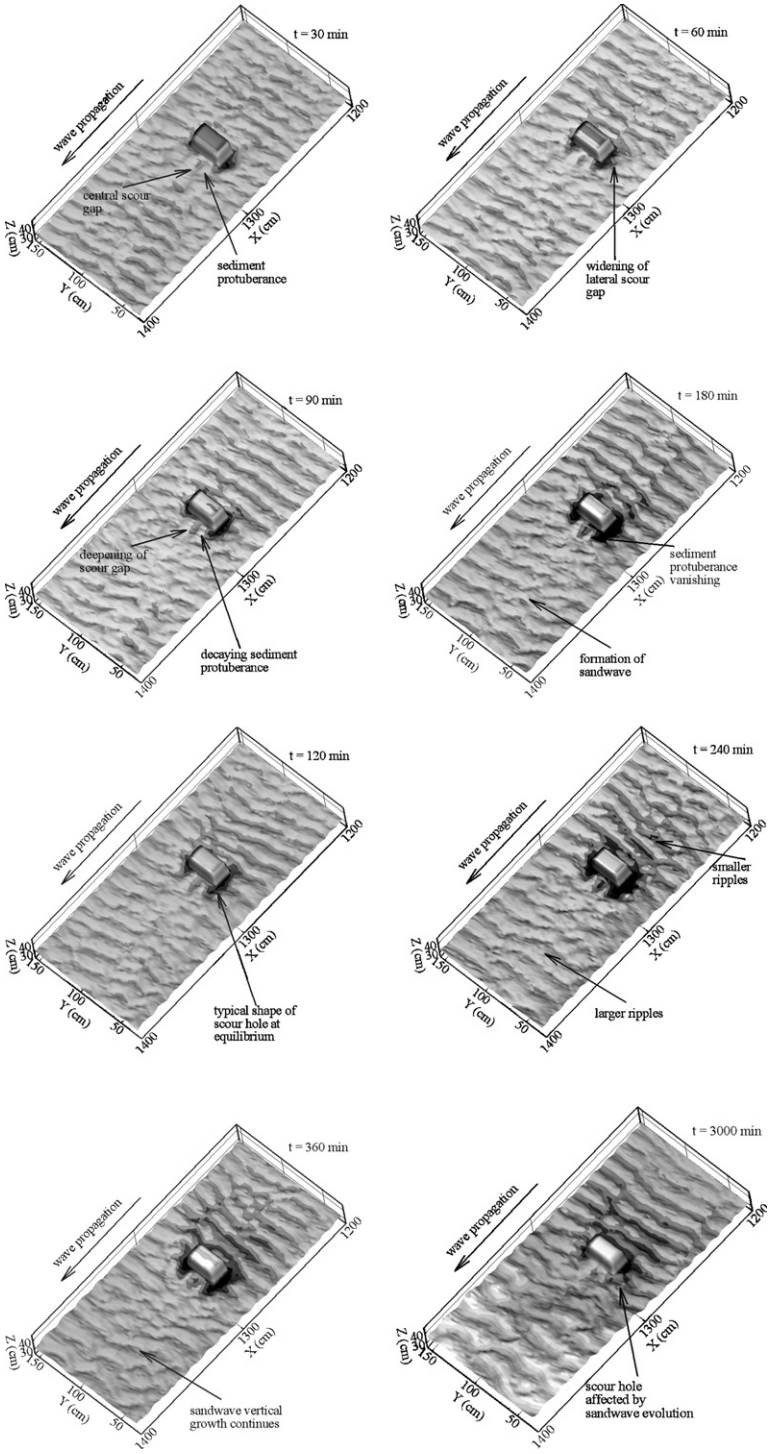

Fig. 12. Evolution over time of scour hole around cylinder 3 (Table 2) under WA with hydraulic conditions: $T_w = 4.1$ s, $H_w = 14.7$ cm, $L_w = 9.4$ m, and $h = 56$ cm.

sandwave, while smaller ripples amalgamate over the trough of the sandwave (Cataño-Lopera and García, 2005). Notice in Fig. 12 that at $t = 360$ min the previously developed sandwave is now more apparent. The cylinder, coincidentally, was placed right in between the crest and the trough of the sandwave. As time increased, the sandwave grew vertically and migrated in the positive x-direction, although very slowly compared to the migration rate of ripples. The sandwave strong effects on the scour pattern around the object can be observed at $t = 3000$ min in Fig. 12. Eventually, the scour hole was almost completely reduced and may have disappeared due to the presence of the sandwave. Periodic burial and un-burial of the cylinder occurred due to the passage of the sandwave.

In such cases, ripples were observed in the very vicinity of the cylinder, since the typical scour hole had already disappeared.

Notice here that the model cylinders used in this study were normally larger than the maximum vertical dimensions of the ever-present ripples. The ripple system was away from the body due to a wash out effect produced by the local acceleration of the flow in the vicinity of the object. This was reflected by the consequent increase of the Shields parameter around the cylinder.

5.3.2. *Flow field around a partially buried cylinder at equilibrium conditions*

Measurements of vertical velocity profiles were performed at 17 locations around the cylinder for the experiment described above. Fig. 13a shows a schematic diagram of the point-measurement distribution around cylinder number 3 (see Table 1). Hydraulic conditions are listed in the caption of Fig. 12. Velocity time series were recorded over 50 wave periods in order to ensure steadiness of the recorded signal. Average values of mean, maximum positive and negative velocities over the vertical were calculated with the help of a post-processing Matlab-based code. Velocities were recorded between $t = 100$ and 240 min, approximately. During this period, the morphology around the cylinder was observed to change very little as can be concluded by observing the contours maps in Fig. 12. Therefore, bed conditions can be considered as quasi-stationary. The bottom profile depicted in Fig. 13b is the result of averaging bottom profiles at $t = 120$ and 240 min.

In the present study, only average values of maximum positive and negative horizontal velocities in the x-direction, U_x, are shown (Fig. 13b). Instantaneous values of the other two components, U_y and U_z, can be used for turbulence computations. For instance, this would enable the study of zones of production and dissipation of turbulent kinetic energy. Knowledge of this quantity, as well as other statistical moments, is of prime importance

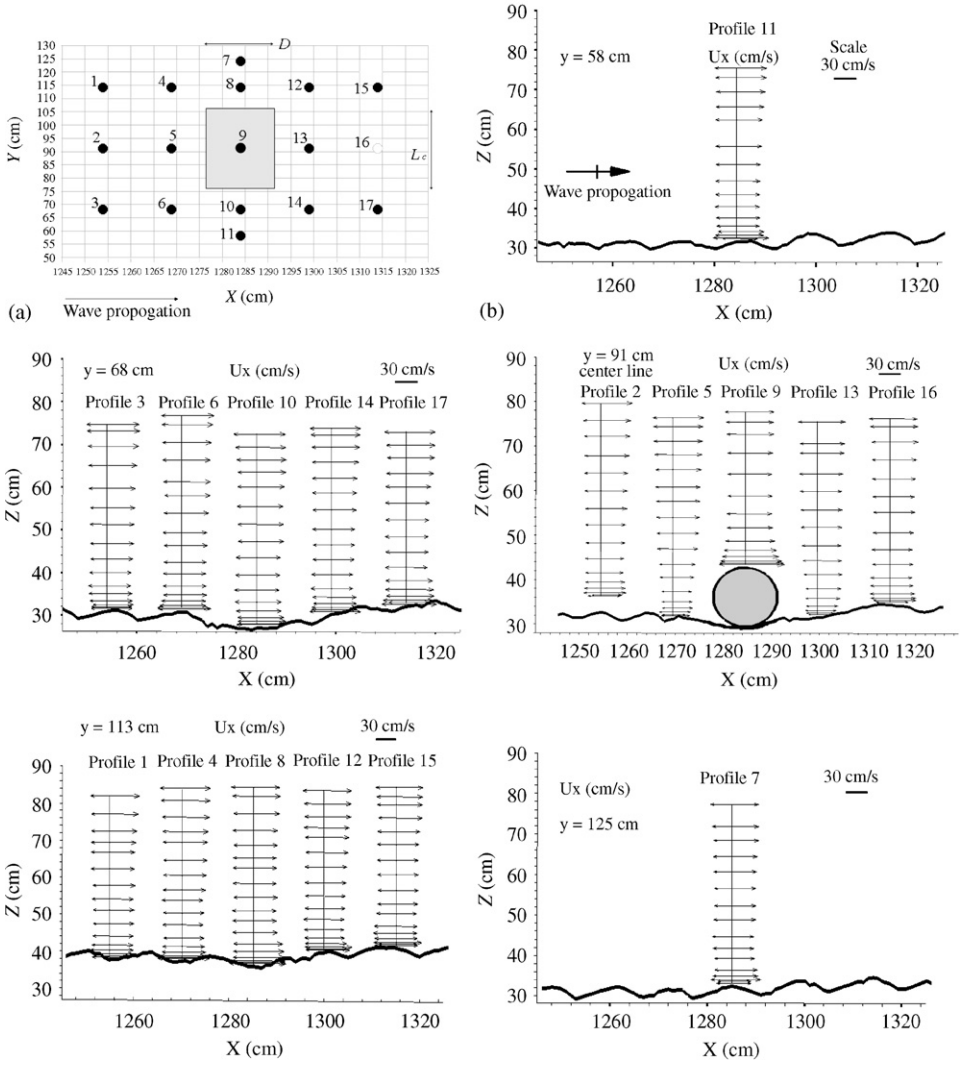

Fig. 13. (a) Schematic diagram of vertical velocity profiles around a partially buried cylinder. (b) Positive and negative velocity profiles around cylinder. Hydraulic conditions as listed in caption of Fig. 12.

for the overall understanding of shear stress distributions around the object. In that way, the sediment transport processes responsible for burial and scour hole development can be better understood. In addition, empirical measurements, as reported herein, are of great importance for posterior calibration and enhancement of any well conceived predictive numerical code.

Notice in Fig. 13b that velocities are higher along the center line of the cylinder in the x-direction than on the lateral edges of the body. Positive velocities are higher in magnitude than negative values (see profiles in Fig. 13b). This explains the fact that the downstream length of the scour hole is greater than its upstream counterpart. Three-dimensional effects are more pronounced at the vicinity of the cylinder which is accompanied by stronger vortex shedding and consequent higher shear stresses. This constitutes the main mechanism under which acceleration of the flow is stronger, thus enhancing the excavation process by bringing sediment into suspension. This is in agreement to what was aforementioned about the shear stress. Via the Shields parameter, the shear stresses are the main generator of scouring, leading to lateral excavation towards the center of the cylinder and hence, inducing settlement of the object. Sediment into suspension is captured and transported by the flow away from the body. This process dictates the shape and size of the scour hole depending on the combined effect of the cylinder aspect ratio, a_r, and the KC number.

6. Conclusions

- The present experimental evidence suggests that higher burial depths correspond to the case when the angle of attack is 90°. For smaller initial angles of attack, perturbation of the flow due to the presence of the body is not as pronounced leading to smaller burial depth. Lower burial depths are obtained when the initial rotation is 0°.
- The equation for prediction of burial due to local scour originally developed for angle of attack 0°, i.e. Eq. (15) developed by Cataño-Lopera and García (2006), is still valid for $\alpha_f > 80°$. For smaller angles of attack, it would be necessary to include the orientation angle, α, in the previous formula.
- Length and width of scour hole around cylinder at equilibrium conditions, for WA and CF, are primarily a function of the Keulegan-Carpenter number, KC, and the cylinder aspect ratio, a_r, through the following empirical relationship: $L_{st}/D = \frac{3}{4}a_r^{3/10}\,KC^{3/5}$. This formula is physically congruent with the governing hydrodynamic conditions and represents a better agreement with the present measured data than other existing formulae.
- At equilibrium conditions, it was observed that the width of the scour hole, W_s/L_c, tended to a stable value of 1.8 regardless the type of flow, i.e. under waves alone or combined flow.
- Scour hole width is also shown to be orientation dependant. This quantity increases with increasing α.
- The final angle of orientation is primarily a function of the Shields parameter, θ. The final orientation, α_f, depends also on the specific density of the cylinder. That is, under similar hydraulic conditions, the final orientation is larger for lighter cylinders than for denser cylinders regardless cylinder characteristics. Cylinders with initial orientations of 0° and 90° did not turn regardless cylinder properties.
- Equilibrium relative burial depth, B_d/D, is also a function of the orientation of the cylinder, α. It was observed that the maximum cylinder burial is for the case of $\alpha = 90°$ while the minimum value correspond to $\alpha = 0°$.
- Most of the scouring around and underneath the object occurs during the first 3–10 min. A continuous increasing of width and length along with cylinder burial was observed. When cylinder diameter is larger that the surrounding bedforms (ripples or sandwaves), local scour dominates the scouring and self-burial processes. After certain time, normally after 120 min starting from flat bed conditions, larger bottom features strongly affect the scour hole geometry, and burial is no longer governed by local scour. As a result, the cylinder may undergo periodic, partial or, total burial due to the passage of the migrating bedform.
- Velocity records around a semi-buried cylinder show features that help to understand the geometric characteristics of the scour hole around the object. Velocity measurements showed that higher velocities acted along the centerline of the cylinder. This, along with vortex shedding and lee-wake effects, is believed to be the main reason behind the fact that the central scour-gap downstream of the cylinder is always bigger than that at the edges of the body.
- When sandwaves interact with cylinder, the scour hole may be reduced until it disappears. During the un-burial process of the cylinder, the scour pattern may return to a similar configuration of that governed by local scour.

Acknowledgements

This work has been funded by the Coastal Geosciences Program of the US Office of Naval Research, Grants N00014-01-1-0337 and N00014-05-1-0083. This support is gratefully acknowledged.

References

Bros, B., 1999. Numerical modeling of flow and scour at pipelines. Journal of Hydraulic Engineering. ASCE 125 (5), 511–523.

Carstens, M.R., Martin, C.S., 1963. Settlement of cylindrical mines into the seabed under gravity waves. Navy Mine Defense Laboratory, Panama City, FL, Final Report Project No. A-628.

Cataño-Lopera, García, M.H., 2005. Burial of short cylinders induced by scour and bedforms under waves plus currents. Proceedings of the World Water and Environmental Resources Conference, ASCE, Alaska,14-19 May.

Cataño-Lopera, Y., García, M.H., 2006. Burial of short cylinders induced by sandwaves and scour under combined waves and currents. Journal of Waterway port-coastal and Ocean Engineering–ASCE, in press.

Cokgor, S., 2002. Hydrodynamics forces on a partly buried cylinder exposed to combined waves and current. Ocean Engineering 29 (7), 753–768.

Hansen, E.A., 1992. Scour below pipelines and cables: A simple model. Proceedings of the 11th Offshore Mechanics and Artic Engineering Conference, ASME, Calgary, Canada, vol. V-A, Pipeline Technology, pp. 133–138.

Li, F., Cheng, L., 1999a. Numerical model for local scour under offshore pipelines. Journal of Hydraulic Engineering–ACSE 125 (4), 400–406.

Li, F., Cheng, L., 1999b. Numerical simulation of pipeline local scour with lee-wake effects. International Journal of Offshore and Polar Engineering 10 (3), 195–199.

Liang, D.L., Cheng, L., Yeow, K., 2005. Numerical study of the Reynolds-number dependence of two-dimensional scour beneath offshore pipelines in steady currents. Ocean Engineering 32, 1590–1607.

Mao, Y., 1988. Seabed scour under pipelines. Proceedings of the Seventh International Conference of Offshore Mechanics and Artic Engineering Conference, ASME, Houston, TX, vol. V, pp. 33–38.

Morelissen, R., Hulscher, S.J.M.H., Knaapen, M.A.F., Németh, A., Bijker, R., 2003. Mathematical modeling of sand wave migration and the interaction with pipelines. Coastal Engineering 48, 197–209.

Smith, H.D., Foster, D.L., 2005. Modeling of flow around a cylinder over a scoured bed. Journal of Waterway Port Coastal and Ocean Engineering–ASCE pp. 14–24.

Snyder, W.H., Castro, P.I., 1999. Accoustic-doppler-velocimeter evaluation in a stratified tank. Journal of Hydraulic Engineering 125 (6), 595–603.

Sumer, B.M., Fredsoe, J., 1990. Scour below pipelines in waves. Journal of Waterway Port Coastal and Ocean Engineering–ASCE 116 (3), 307–323.

Sumer, B.M., Fredsoe, J., 1996. Scour around pipelines in combined waves and current. Proceedings of the Seventh International Conference on Offshore mechanics and Artic Engineering Conference, ASME, Florence, Italy, Vol. V, Pipeline Technology, pp. 595–602.

Sumer, B.M., Truelsen, C., Sichmann, T., Fredsoe, J., 2001. Onset of scour below pipelines and self-burial. Coastal Engineering 42, 313–335.

Sumer, B.M., Fredsoe, J., 2002a. The mechanics of scour in the marine environment. Advanced Series on Ocean Engineering, Vol. 17. World Scientific, Teaneck, NJ., USA.

Sumer, B.M., Fredsoe, J., 2002b. Hydrodynamics around cylindrical structures. Advanced Series on Ocean Engineering, Vol. 12. World Scientific, Teaneck, NJ., USA.

Swart, D.H., 1974. Offshore sediment transport and equilibrium beach profiles, Delft Hydraulics Lab. , Publ 131.

Voropayev, S.I., Cense, A.W., McEachern, G.B., Boyer, D.L., Fernando, H.J.S., 1999. Dynamics of sand ripples and burial/scouring of cobbles in oscillatory flow. Applied Ocean Research 21 (5), 249–261.

Voropayev, S.I., Testik, F.Y., Fernando, H.S.J., Boyer, D.L., 2003. Burial and scour around a short cylinder under progressive shoaling waves. Coastal Engineering 30, 1647–1667.